iJRASET
International Journal For Research in Applied Science and Engineering Technology

INTERNATIONAL JOURNAL FOR RESEARCH

IN APPLIED SCIENCE & ENGINEERING TECHNOLOGY

Volume: 9 **Issue:** VI **Month of publication:** June 2021

DOI: https://doi.org/10.22214/ijraset.2021.34856

www.ijraset.com

Call: 08813907089 | E-mail ID: ijraset@gmail.com

International Journal for Research in Applied Science & Engineering Technology (IJRASET)
ISSN: 2321-9653; IC Value: 45.98; SJ Impact Factor: 7.429
Volume 9 Issue VI Jun 2021- Available at www.ijraset.com

Structural, Magnetic and Dielectric Analysis of Higher Magnetic Mn Doped Zn-Cr Oxide Nanoparticles

S. D. Balsure[1], V. D. More[2], S. S. Kadam[3], K. P. Haval[4], A. B. Kadam[5]
[1, 5]*Department of Physics, Jawahar College, Anadur, Dist. Osmanabd (M.S.) India*
[2]*Department of Physics, Rajarshi Shahu College, Pathrai, Dist. Auranagabad, (M.S.) India*
[3]*Department of Physics, Shrikrishna Mahavidyalaya, Gunjoti, Dist. Osmanabad, (M.S.) India*
[4]*Department of Chemistry, Dr. B. A. M. University, Sub-campus Osmanabad, (M.S.) India*

Abstract: ***Higher magnetic Mn doped Zn-Cr oxide nanoparticles with general compositional formula $M_xZn_{0.95-x}Cr_{0.05}O$ have been synthesized by using sol-gel auto combustion technique. Room temperature X-ray diffraction (XRD) technique has been employed to study the structural and microstructural parameters of the as-prepared samples. XRD analysis confirms the phase purity and hexagonal wurtzite structure of all the samples. Replacement of Zn^{2+} ions by Mn^{2+} ions shifts peak positions slightly towards the lower angles which in turn expands the lattice lengths 'a' from 3.2487 to 3.2528 Å and 'c' from 5.2043 to 5.2118 Å. Crystallite size obtained from Scherrer equation was confirmed by Williamson – Hall (W-H) and size – strain plot methods (SSP). Both W-H and SSP methods reveals the tensile type strain for undoped sample and comprehensive type strain for Mn^{2+} doped samples. Magnetic properties were investigated by using vibrating sample magnetometer. Diluted ferromagnetic behaviour is observed for all the samples and saturation magnetization (M_S) increases from 0.0514 to 0.1163 emu/gm. Two-probe technique was employed to understand the dielectric behaviour of the samples as a function of frequency. At lower frequency region, both dielectric constant (ε′) and dielectric loss tangent (tan δ) shows higher values and decreases with the increasing applied frequency.***

Keywords: Sol-gel technique, W-H analysis, SSP method, ferromagnetism, dielectric constant.

I. INTRODUCTION

Materials with nano dimensions due to their large surface to volume ratio, shows altered physic-chemical properties as compared to the bulk materials [1-3]. Semimagnetic semiconductors (SMSC) are the semiconducting materials which are characterized by the random substitution of a fraction of the host atoms by magnetic atoms having high magnetic moments. These materials are lies at the interface between magnetic and semiconducting materials and are termed as Dilute Magnetic Semiconductors (DMS). DMS's, in-particular, can be fractionally replaced by transition metal (TM) ions or rare earth (RE) ions in order to obtain the controlled diluted magnetic behaviour [4, 5]. Strong coupling between conduction and valence bands of the host SC electron states of magnetic ions is the key feature of DMS's. Due to this coupling, magnetic ions within the DMS's are allow to reconcile the influence of an external magnetic field. Spin alignment of magnetic ions due to external magnetic field generated the effective exchange field which acts on the spins of band electrons. This is the way through which the influence of magnetic field on SC's can be amplified by magnetic ions. In the beginning of 1980's, researchers have initiated the research on semiconductors by introducing Mn ions. The random distribution of TM or RE ions in DMS's crystal lattice leads to novel magnetic parameters such as low temperature spin-glass like phase formation, Zeeman splitting of electron levels, extremely high Faraday rotation, metal-insulator transition induced by magnetic field etc. [6]. These semiconductors are envisioned to be potential building blocks for spintronic devices.

Recently, transition metal (TM)-doped semiconductors are receiving theoretical and experimental attention because of their optical and magnetic properties. For example, TM-doped zinc oxide (ZnO) semiconductors. ZnO based magnetic semiconductors have attracted much attention for their promising versatile applications such as spintronic, optoelectronic and piezoelectronic materials [7]. Substitution of proper dopant with proper concentration and synthesis conditions controls the physical properties of ZnO nanostructures such as structural, micro-structural, magnetic, and dielectric behaviour. Higher magnetic ions substitution in ZnO crystals, improves the room temperature ferromagnetic behaviour. Pure and doped ZnO nanocrystals can be obtained by several synthesis routs, among which sol-gel is one of the best method [8-10]. This method is cost effective and requires relatively low temperature for nano-particle formation

In the present work, we have synthesized the Mn^{2+} doped Zn-Cr oxide nanoparticles by sol-gel auto-combustion method. Structural parameters were investigated by using X-ray diffraction patterns collected at room temperature.

Bragg's peak widths and peak positions were used to estimate the crystallite size and micro-strain induced in the crystal lattice by using Scherrer, W-H and SSP methods. Uniform deformation model (UDM), uniform stress deformation model (USDM) and uniform deformation energy density model (UDEDM) were considered for the W-H analysis of the samples. Magnetic properties of the samples were investigated by using vibrating sample magnetometer and frequency dependent dielectric properties were investigated by using two-probe technique.

II. EXPERIMENTAL

Mn doped oxide nanoparticles of $Mn_xZn_{0.95-x}Cr_{0.05}O$ (x = 0.0, 0.02, 0.04, 0.06, 0.08 and 0.1) were obtained by using sol-gel technique. Metal nitrates (A. R. grade) with high purity (>98.5% pure) $Mn(NO_3)_2{\cdot}H_{12}O_6$, $Zn(NO_3)_2{\cdot}H_{12}O_6$, $Cr(NO_3)_3{\cdot}H_{18}O_9$ and citric acid were used as initial materials. Sufficient amount of double distilled water was taken to dissolve the initial materials with their weight proportion in the composition. Whole mixture was stirred continuously at a constant temperature of 90 ^{0}C. Chelating agent, citric acid, was mixed with the nitrates solution by the metal nitrate to citrate ratio of 1:3. Addition of liquid ammonia with slow rate kept the pH of the solution at 7. Continuous stirring with constant heating and by maintain the neutral pH nearly for 2 to 3 hours converts the mixture in to viscous gel. After half an hour the dark brown gel was burnt by self – ignition process and converted into brown ash. The final powders were obtained by grinded ash powders finally sintered at 900^{0}C for 6 hours. The as-prepared samples were characterized by X-ray diffraction technique, Vibrating sample magnetometer and two-probe technique for their micro-structural, magnetic and dielectric investigations. All the XRD patterns were recorded on Regaku (Miniflux II) diffractometer with Cu-Kα radiation (1.5406 ´) operated at 40 kV within the 2θ range of 20 to 80^0. Magnetic measurements were carried out by applying the magnetic field up-to 15KOe on a vibrating sample magnetometer. Disc shaped samples with silver paste were used to understand the dielectric behaviour of the samples within the frequency range 50Hz to 50MHz by using Hioki HiTESTER 3532-50.

III. RESULTS AND DISCUSSION

Well indexed Bragg's lines for the planes (100), (002), (101), (102), (110), (103), (200), (112), (201), (004) and (202) as shown in Fig. 1 indicates the phase purity of $Mn_xZn_{0.95-x}Cr_{0.05}O$. Broad Bragg's lines indicate nano-crystalline nature of the samples. All the planes indexed by Miller indices are corresponds to the hexagonal wurtzite structure of the samples with space group P63 m c and indexed to standard crystallographic open database card No. 90-901-1663 corresponds to zinc oxide [11].

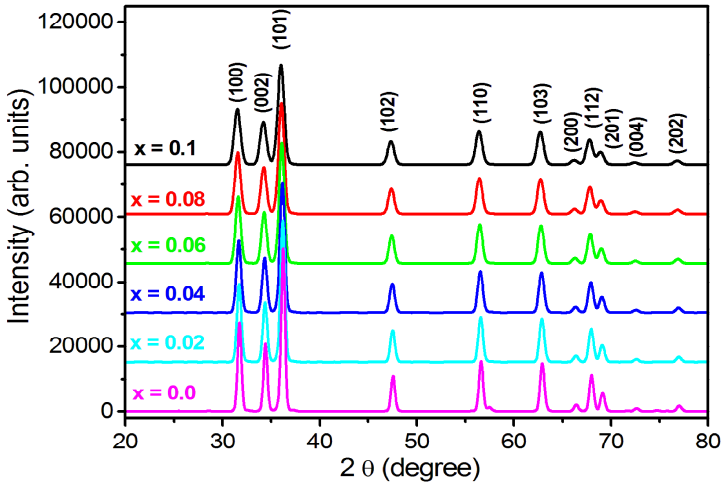

Fig. 1: XRD patterns of $Mn_xZn_{0.95-x}Cr_{0.05}O$

Close observation of X-ray patterns shows that the peak positions slightly shifted towards lower angles with the addition of Mn^{2+} ions in Zn-Cr-O crystal lattice. Also, it can be seen that the peak height decreases and peak width increases with the substitution of Mn^{2+} ions. Lattice parameter 'a' and 'c' for the hexagonal structure were computed by using the following relation [12];

$$\frac{1}{d^2} = \frac{4}{3}\left(\frac{h^2 + hk + k^2}{a^2}\right) + \frac{l^2}{c^2} \qquad (1)$$

Where, d-is interplaner spacing's, hkl-are the miller indices and 'a' and 'c' are the lattice parameters. It can be seen from Table 1 that the insertion of Mn^{2+} ions in Zn-Cr-O crystal lattice enhances the lattice lengths 'a' from 3.2487 to 3.2528 Å and 'c' from 5.2043 to 5.2118 Å. This expansion of lattice parameters is attributed to the ionic radii differences of Mn^{2+} (0.89 Å) and Zn^{2+} (0.83 Å) [13]. Cell volume computed by using the relation $V = 0.866a^2c$ is obtained increasing with the addition of Mn^{2+} ions which is analogues with the increasing behaviour of lattice parameters. The distortion factor 'u' for the samples possessing wurtzite structure is obtained by using the following relation [14];

$$u = \left[\frac{a^2}{3c^2} + 0.25\right] \qquad (2)$$

As reported in the literature, distortion factor 'u' represents the displacement of each atom with respect to next one along 'c' axis. The standard reported value of distortion factor for wurtzite ZnO crystal lattice is (0.379) and in the present case; obtained distortion factor is very close to the standard value (0.380) [15].

Simple mass-volume relation $d_{Bulk} = M/\left(\pi r^2 h\right)$; was used to obtain the bulk density (d_B) values and X-ray density was obtained by using the relation discussed elsewhere [16]. Bulk density of the samples increases from 4.677 to 4.830 gm/cc whereas, X-ray density decreases from 5.639 to 5.544 gm/cc with the addition of Mn^{2+} ions (Table 1). Porosity in percentage of the samples was obtained by using the following relation [16];

$$P(\%) = \left(\frac{d_X - d_{Bulk}}{d_X}\right) \times 100 \qquad (3)$$

Table 1 indicates that the porous nature of the sample decreases from 20.50 to 14.85 % with the increasing concentration of Mn^{2+} ions in Zn-Cr-O crystal lattice. The specific surface area 'S' obtained by using the relation discussed in literature [17] increases from 73 to 111 m^2/gm with the addition of Mn^{2+} ions.

TABLE I

Lattice parameters (a, c), c/a ratio, unit cell volume (V), distortion factor 'u', X-ray density (d_X), bulk density (d_B), porosity (P) and specific surface area (S) for $Mn_xZn_{0.95-x}Cr_{0.5}O$

'x'	Lattice parameter (Å)			'V' $(Å)^3$	'u'	'd_X' (gm/cc)	'd_B' (gm/cc)	'P' (%)	'S' (m^2/gm)
	'a'	'c'	c/a						
0.0	3.2487	5.2043	1.602	47.57	0.380	5.639	4.677	20.50	73
0.02	3.2494	5.2070	1.602	47.61	0.380	5.619	4.718	19.09	81
0.04	3.2503	5.2093	1.602	47.66	0.380	5.599	4.747	17.94	87
0.06	3.2510	5.2102	1.602	47.69	0.380	5.581	4.790	16.50	93
0.08	3.2517	5.2110	1.602	47.72	0.380	5.563	4.830	15.17	100
0.1	3.2528	5.2118	1.602	47.76	0.380	5.544	4.827	14.85	111

Well known Scherrer equation was used to estimate the average crystallite size of the samples [12];

$$t_{311} = \frac{K\lambda}{\beta_{FWHM}\mathrm{Cos}\theta_B} \qquad (4)$$

Where, K is crystallographic constant (K~0.9), λ-is incident wavelength (1.5406 Å), β_{FWHM} - Full width at half of its maximum and θ_B - is Bragg's position. Table 2 represents the values of average crystallite size ranging from 17.71 to 11.18 nm with the addition of Mn^{2+} ions in Cr-Zn-O nanocrystals.

ISSN: 2321-9653; IC Value: 45.98; SJ Impact Factor: 7.429
Volume 9 Issue VI Jun 2021- Available at www.ijraset.com

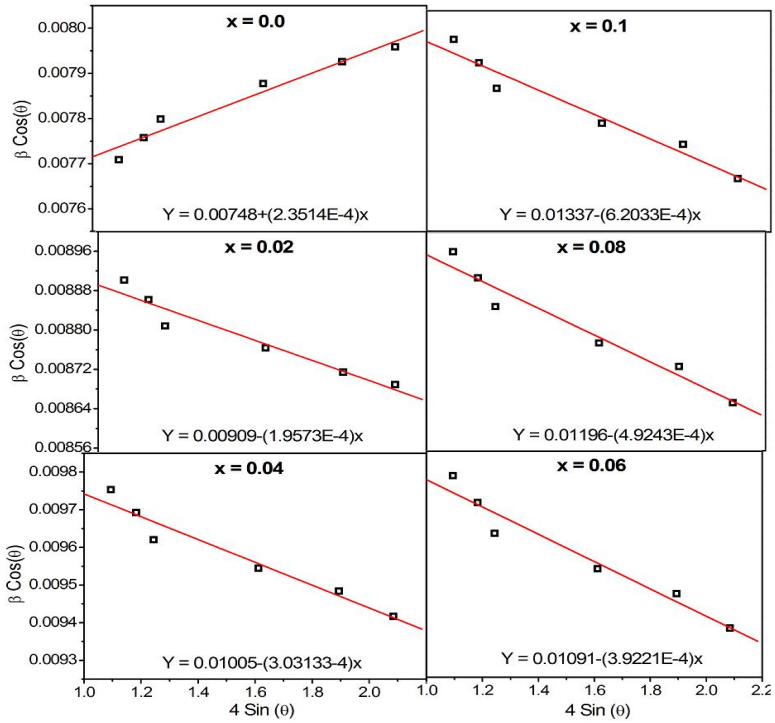

Fig. 2: UDM plots of $Mn_xZn_{0.95-x}Cr_{0.05}O$

More accurate way to estimate the crystallite size is to consider the strain induced in the crystal lattice. Scherrer equation is modified in the Williamson- Hall method in which the strain induced in the crystal lattice was considered. The analysis of XRD line broadenings provides the more accurate information of size and shape of the nanocrystals. Uniform deformation model (UDM) was assumed to estimate the crystallite size and lattice strain by using the modified W-H equation [18];

$$\beta Cos\theta = 4\varepsilon Sin\theta + \frac{k\lambda}{t_{W-H}} \qquad (5)$$

Fig. 2 represents the UDM plots of $Mn_xZn_{0.95-x}Cr_{0.05}O$. Slope of the linearly fitted lines for the plots drawn between 4 sin (θ) along x-axis and β cos (θ) along y-axis gives the micro-strain induced in the crystal lattice and the y-intercept gives the crystallite size of the samples. For the Mn-free sample the positive value of the strain is observed which indicates the tensile type of strain. While as for Mn-doped samples negative values of strain are observed which indicates the comprehensive type of strain induced in the crystal lattice. The variation comprehensive type strain in the Mn-doped Zn-Cr-O crystals is analogues with the variation of lattice parameters. Crystallite size obtained from y-intercepts of UDM plots varies from 19.36 to 10.83 nm which is in good agreement with the values obtained from Scherrer equation.

TABLE II
Crystallite size (t) and strain induced in $Mn_xZn_{0.95-x}Cr_{0.05}O$

'x'	Scherrer	W-H Analysis						SSP Method	
	't' (nm)	UDM		USDM		UDEDM		't' (nm)	$\varepsilon\times10^{-3}$
		't' (nm)	$\varepsilon\times10^{-4}$	't' (nm)	$\varepsilon\times10^{-4}$	't' (nm)	$\varepsilon\times10^{-4}$		
0.0	17.71	19.36	2.35	19.28	2.20	19.33	2.26	19.32	6.49
0.02	15.77	15.93	-1.96	15.97	-1.81	15.95	-1.89	15.99	-6.13
0.04	14.47	14.41	-3.03	14.47	-2.79	14.44	-2.93	14.53	-7.56
0.06	13.45	13.27	-3.92	13.32	-3.61	13.30	-3.78	13.43	-8.74
0.08	12.39	12.11	-4.92	12.17	-4.53	12.14	-4.74	12.29	-10.06
1.0	11.18	10.83	-6.20	10.89	-5.70	10.86	-5.97	11.03	-11.76

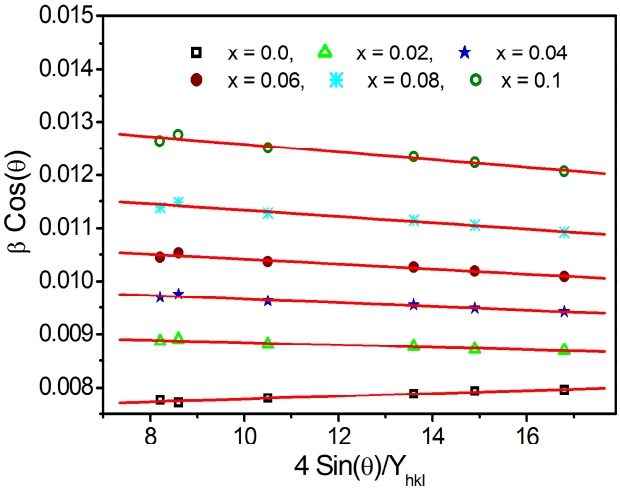

Fig. 3: USDM plots of $Mn_xZn_{0.95-x}Cr_{0.05}O$

Isotropic nature of line broadenings is also assumed in another model, uniform stress deformation model (USDM). As described by Hook's law, a linear proportionality have been observed in the stress and strain given by the equation $\sigma = Y\varepsilon$ (where, σ - is stress, ε - is strain and Y – is Young's modulus) [19] and the modified equation can be written as;

$$\beta_{hkl}Cos\theta = \frac{k\lambda}{t} + \frac{4\sigma Sin\theta}{Y_{hkl}} \qquad (6)$$

In the above equation, Young's modulus (Y_{hkl}) for hexagonal crystal structures are obtained by using the relation discussed in literature [20]. Slopes of linearly fitted USDM plots (Fig. 3) gives the values of uniform stress, and y-intercepts gives the crystallite sizes.

Both the UDM and USDM methods are based on the assumption of isotropic nature of crystals. Furthermore, most of the hexagonal crystals unable not justify the uniform strain distribution in all crystallographic directions. Hence, the linearity between stress and strain relation is no longer independent. The energy density 'u' can be considered for the estimation of strain by using the relation $u = \varepsilon^2 Y_{hkl}/2$ and the equation (6) can be improved as;

$$\beta_{hkl}Cos\theta = \frac{K\lambda}{t} + 4Sin\theta\left(\frac{2u}{Y_{hkl}}\right)^{1/2} \qquad (7)$$

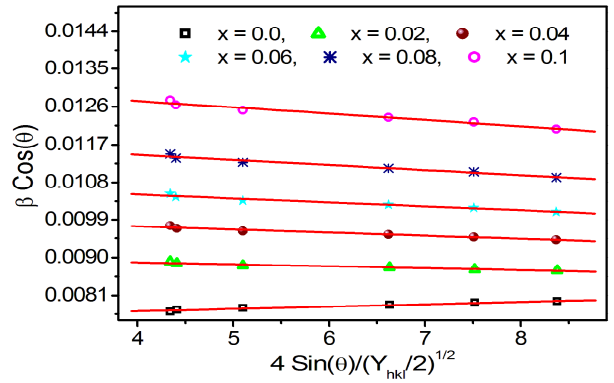

Fig. 4: UDEDM plots of $Mn_xZn_{0.95-x}Cr_{0.05}O$

Linearly fitted UDEDM lines plotted between $4Sin\theta(2u/Y_{hkl})^{1/2}$ versus $\beta_{hkl}Cos\theta$ are shown in Fig. 4. Uniform deformation density was estimated from the slope and y-intercepts give the crystallite size. Uniform deformation density was related to the lattice stress by the relation $u = \sigma^2/Y_{hkl}$ through the strain can be obtained.

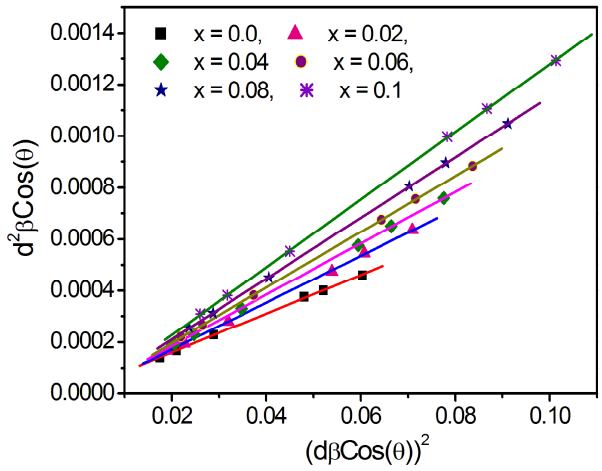

Fig. 5: SSP plots of $Mn_xZn_{0.95-x}Cr_{0.05}O$

Isotropic nature of line widths is assumed in W-H analysis which implies that the diffraction domains are also in isotropic nature [21]. Better knowledge of size and strain can also be obtained from size-strain plot method (SSP) which gives less weightage for the reflections occurred at higher angles where the accurateness is comparatively lesser. In this method, crystallite size is described by assuming the Lorentz's function and strain profile is obtained by assuming the Gaussian function. Size and strain by SSP method can be obtained by using following relation [22];

$$\left(d_{hkl}\beta_{hkl}Cos\theta\right)^2 = \frac{k\lambda}{t_{SSP}}\left(d_{hkl}^2\beta_{hkl}Cos\theta\right) + \left(\frac{\varepsilon}{2}\right)^2 \qquad (7)$$

Fig. 5 shows the linearly fitted SSP graphs plotted between $\left(d_{hkl}^2\beta_{hkl}Cos\theta\right)$ and $\left(d_{hkl}\beta_{hkl}Cos\theta\right)^2$ for all the samples of Mn doped Zn-Cr oxide nanoparticles. Slopes of these straight lines give crystallites sizes and Y-intercept gives lattice strains as listed in Table 2. Crystallite size and lattice strain obtained from Scherrer, W-H analysis and SSP method are found in good agreement with each other.

M-H hysteresis curves of $Mn_xZn_{0.95-x}Cr_{0.05}O$ nanoparticles recorded at room temperature are shown in Fig. 6 (a). Hysteresis curves imply that the Mn-free and Mn-doped samples possess diluted ferromagnetic behaviour at room temperature. For undoped sample saturation magnetization (M_S) is observed M_S = 0.0514 emu/g which found increases up to 0.1163 emu/gm for the highest doping of Mn^{2+} ions. Fig. 6 (b) shows the variation of saturation magnetization (M_S) and coercivity (H_C) as a function Mn doping in Zn-Cr-O crystal lattice. Coercivity of the samples decreases from 338 Oe to 112 Oe with Mn addition.

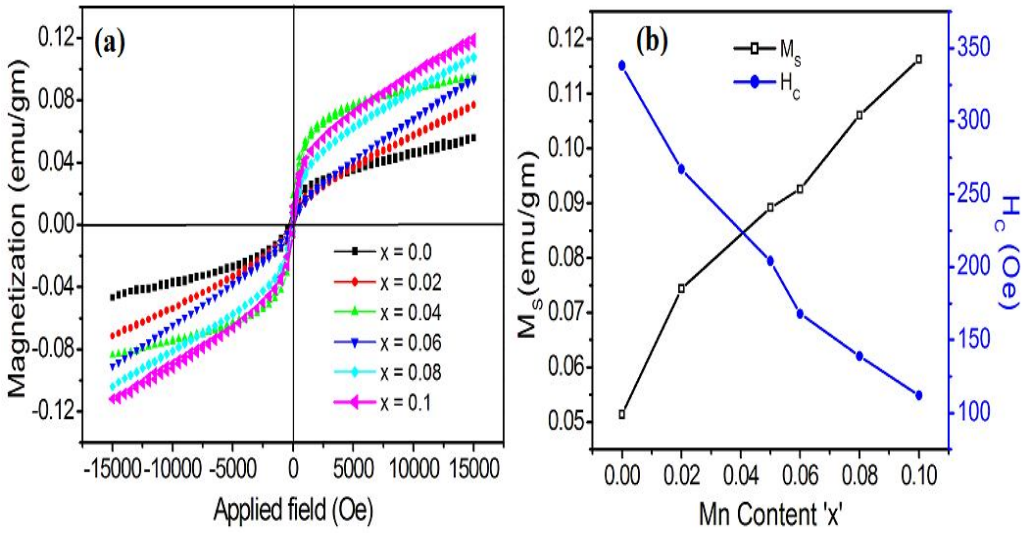

Fig. 6: (a) M-H hysteresis curves and (b) variation of saturation magnetization (M_S) and coercivity (H_C) for $Mn_xZn_{0.95-x}Cr_{0.05}O$

Fig. 7 (a, and b) respectively shows the variation of dielectric constant (ε′) and dielectric loss tangent (tan δ) as a function of frequency within the range 50 Hz to 5 MHz. Typical semiconducting behaviour is obtained for all the samples in which both dialectic constant and loss tangent shows maximum values at lower frequencies and becomes almost constant after decreasing at high frequencies. The polarization effects observed at atomic, ionic, electronic and interfacial level justifies the variation of variation of dielectric constant [23]. It is also observed that insertion of Mn^{2+} ions in Zn-Cr-O crystal lattice increases the values of dielectric constant and dielectric loss tangents.

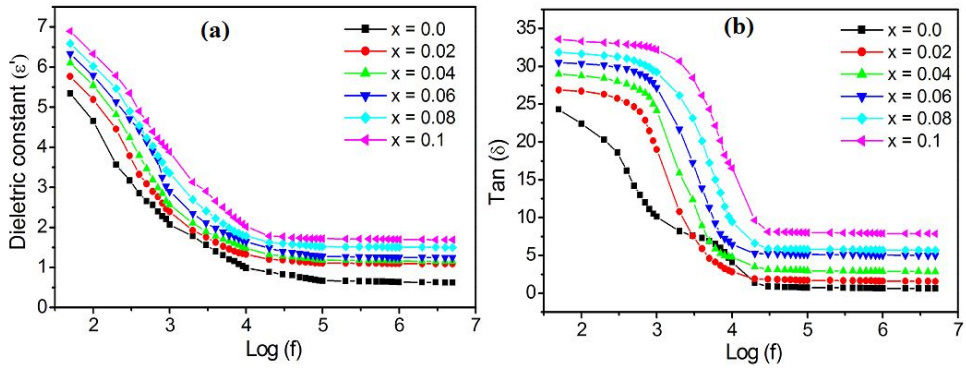

Fig. 7: (a) Variation of dielectric constant (ε′) and (b) variation of dielectric loss tangent (tan δ) as a function of applied frequency for $Mn_xZn_{0.95-x}Cr_{0.05}O$

IV. CONCLUSIONS

Sol-gel synthesis rout successfully produces the oxide nanoparticles of $Mn_xZn_{0.95-x}Cr_{0.05}O$. Well indexed Bragg's lines of XRD patterns confirm the hexagonal wurtzite structure of the samples. No traces of secondary phases are observed which implies that Mn^{2+} ions successfully incorporated in the Zn-Cr-O crystal lattice. Lattice parameters 'a' and 'c' are found increasing with the addition of Mn^{2+} ions. W-H analysis indicates that the Mn^{2+} substituted samples shows comprehensive type strain induced in the crystal lattice. Crystallite size and lattice strain obtained from Scherrer, UDM, USDM, UDEDM and SSP methods are in good agreement with each other. Room temperature intrinsic ferromagnetism is observed in Mn^{2+} - free and doped samples. Dielectric constant is observed higher at lower frequency level and lower for higher frequency level.

REFERENCES

[1] R. H. Kadam, A. Karim, A. B. Kadam, A. S. Gaikwad, S. E. Shirsath, "Influence of Cr^{3+} substitution on the electrical and magnetic properties of $Ni_{0.4}Cu_{0.4}Zn_{0.2}Fe_2O_4$ nanoparticles," Inter. Nano. Lett. vol. 2 pp. 28-34, Oct. 2012.
[2] R. Elilarassi, G. Chandrasekaran, "Synthesis and optical properties of Ni-doped zinc oxide nanoparticles for optoelectronic applications," Opt. Lett. vol. 6, pp. 6-10, April 2010.
[3] R. H. Kadam, K. Desai, V. S. Shinde, M. Hashim, S. E. Shirsath, "Influence of Gd^{3+} ion substitution on the $MnCrFeO_4$ for their nanoparticle shape formation and magnetic properties," J. Alloy. Comp. vol. 657, pp. 487-494, March 2016.
[4] J. A. Jai, "Semimagnetic semiconductors" Comp. Semi. Sci. Techn. vol. 2, pp. 95-102, Feb. 2011.
[5] S. B. Rana, R. P. P. Singh, "Investigation of structural, optical, magnetic properties and antibacterial activity of Ni-doped zinc oxide nanoparticles," J. Mater. Sci. Mater. Electr. vol. 27, pp. 9346-9355, May 2016.
[6] S. Lee, M. Dobrowolska, J. K. Furdyna, Epitaxial II-VI semiconductor quantum structures involving dilute magnetic semiconductor," Woodhead Publishing Series in Elect. Opt. Mater. pp. 153-187, 2020.
[7] M. Kaur, P. Kaur, G. Kaur, K. Dev, P. Negi, R. Sharma, "Structural, morphological and optical proeprties of Eu-N co-doped zinc oxide nanoparticles synthesized using co-precipitation technique," Vacuum, vol. 155, pp. 689-695, Sept. 2018
[8] A. K. Zak, R. Razali, WH A. Majid, M. Darroudi; "Synthesis and characterization of narrow size distribution of zinc oxide nanoparticles," Int. J. Nano. vol. 6, pp. 1399-1403, Jul. 2011.
[9] S. K. Gurav, S. E. Shirsaht, R. H. Kadam, S. M. Patange, K. S. Lohar, D. R. Mane, "Less magnetic and larger Zr^{4+}-Zn^{2+} ions co-substituted structural and magnetic properties of ordered $Li_{0.5}Fe_{2.5}O_4$ nanoparticles," Mater. Res. Bull. 48 (2013) 3530.
[10] S. Liu, H. Sun, A. Suvorova, S. Wang, "One pot hydrothermal synthesis of ZnO – reduced graphane oxide composites using Zn powders for enhanced photocatalysts," Chem. Engg. J. vol. 229, pp. 533-539, Aug. 2013.
[11] Y. N. Xu, W. Y. Ching, "Electronic, optical, and structural properties of some wurtzite crystals," Physical Review B, vol. 48, pp. 4335-4342, Aug. 1993.
[12] S. S. Satpute, S. R. Wadgane, S. R. Kadam, D. R. Mane, R. H. Kadam, "Y^{3+} substituted Sr-hexaferrites: sol-gel synthesis, structural, magnetic and electrical characterization," Ceramica; vol. 65, pp. 274-283, Jun. 2019.
[13] S. J. Haralkar, R. H. Kadam, S. S. More, S. E. Shirsath, M. L. Mane, S. Patil, D. R. Mane, "Intrinsic magnetic, structural and resistivity properties of ferromagnetic $Mn_{0.5}Zn_{0.5}Al_xFe_{2-x}O_4$ nanoparticles," Mater. Res. Bull. vol. 48, pp. 1189, Mar. 2013.

[14] P. S. Sundaram, T. Sangeetha, S. Rajakarthihan, R. Vijayalakshmi, A. Elangovan, G. Arivazhagan, "XRD structural studies on cobalt doped zinc oxide nanoparticles synthesized by coprecipitation method; Williamson-Hall and size – strain ploat approaches," Physica B: Cond. Mater. vol. 595, pp. 412342, Oct. 2020.
[15] P. Bindu, S. Thomas, "Estimation of lattice strain in ZnO nanoparticles: X-ray peak profile analysis," J. Theor, Appl. Phys. vol.8, pp. 123-134, Mar. 2014.
[16] S. S. Satpute, S. R. Wadgane, K. Desai, D. R. Mane, R. H. Kadam, Substitution of Y^{3+} ions on the structural, magnetic and electrical properties of cobalt ferrite nanoparticles," Ceramica vol. 66, pp. 66-69, Mar. 2020.
[17] K. R. Desai, S. T. Alone, S. R. Wadgane, S. E. Shirsath, K. M. Batoo, A. Imran, E. H. Raslan, M. Hadi, M. F. Ijaz, R. H. Kadam, "X-ray diffraction based Williamson-Hall analysis and Rietveld refinement for strain mechanism in Mg-Mn co-substituted $CdFe_2O_4$ nanoparticles," Physica B: Cond. Mater. vol. 614, pp. 413054, Aug. 2021.
[18] K. V. Chandekar, K. M. Kant, "Size-strain analysis and elastic properties of $CoFe_2O_4$ nanoplatelets by hydrothermal method," J. Mole. Stru. vol. 1154, pp. 418-427, Feb. 2018.
[19] A. K. Zak, W. H. Majid, M. E. Abrishami, R. Yousefi, "X-ray analysis of ZnO nanoparticles by Williamson – Hall and size-strain plot methods," Solid State Sci. vol. 13, pp. 251-256, Jan.2011.
[20] J. F. Nye; Physical properties of crystals: Their representation by tensor and matrices; Oxford, New York, 1985.
[21] H. Irfan, M. Radik, S. Anand, "Microstructural evaluation of $CoAl_2O_4$ nanoparticles by Williamson-Hall and size – strain plot methods," J. Asian Ceram. Soc. vol. 6 , pp. 54-62, Jan. 2018.
[22] M. A. Tagliente, M. Massaro, "Strain-driven (002) preferred orientation of ZnO nanoparticles in ion-implanted silica," Nucl. Intst. Meth. Phys. Res. B, vol. 266, pp. 1055-1061, April 2008.
[23] M. Kamran, M. A. Rehman, "Enhanced transport properties in Ce doped cobalt ferrite nanoparticles for resistive RAM applications," J. Alloy. Comp. vol. 822, pp. 153583, May. 2020.

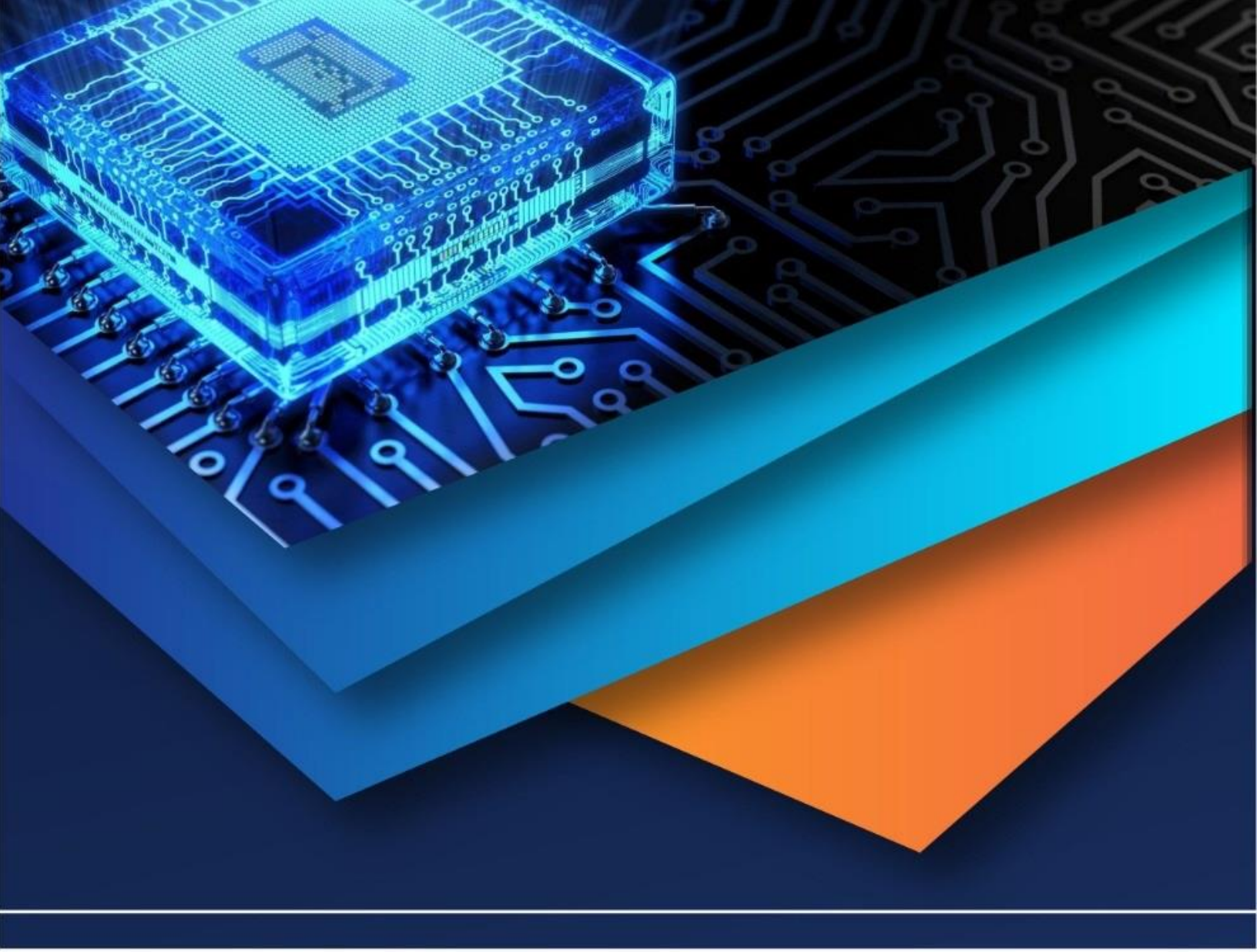

10.22214/IJRASET

45.98

IMPACT FACTOR: 7.129

IMPACT FACTOR: 7.429

INTERNATIONAL JOURNAL FOR RESEARCH

IN APPLIED SCIENCE & ENGINEERING TECHNOLOGY